

Assessment of a quantum phase gate operation based on nonlinear optics

S. Rebić,* and C. Ottaviani, G. Di Giuseppe, D. Vitali and P. Tombesi
Dipartimento di Fisica, Università di Camerino, I-62032 Camerino (MC), Italy

We analyze in detail the proposal for a two-qubit gate for travelling single-photon qubits recently presented by C. Ottaviani *et al.* [Phys. Rev. A **73**, 010301(R) (2006)]. The scheme is based on an ensemble of five-level atoms coupled to two quantum and two classical light fields. The two quantum fields undergo cross-phase modulation induced by electromagnetically induced transparency. The performance of this two-qubit quantum phase gate for travelling single-photon qubits is thoroughly examined in the steady-state and transient regimes, by means of a full quantum treatment of the system dynamics. In the steady-state regime, we find a general trade-off between the size of the conditional phase shift and the fidelity of the gate operation. However, this trade-off can be bypassed in the transient regime, where a satisfactory gate operation is found to be possible, significantly reducing the gate operation time.

PACS numbers: 03.67.Mn, 42.50Gy, 42.65.-k

I. INTRODUCTION

A promising system for quantum computation is to use single photons to encode quantum information [1]. This is due to the photon's robustness against decoherence and the availability of single-qubit operations. However, it is difficult to realize the necessary two-qubit operations since the physical interaction between photons is very small. Linear optics quantum computation [2] and nonlinear optical processes involving few photons have been proposed to circumvent this problem. The first is a probabilistic scheme implicitly based on the nonlinearity hidden in single-photon detectors, while the second is based on the enhancement of photon-photon interaction either in cavity QED configurations [3] or in dense atomic media exhibiting electromagnetically induced transparency (EIT) [4]. In this latter case, optical nonlinearities can be produced when EIT is disturbed, either by introducing additional energy level(s) [6, 7], or by mismatching the probe and control field frequencies [8, 9].

The scope of this paper is to assess the performance of a two-qubit quantum phase gate (QPG) for travelling single photon qubits [10, 11, 12, 13, 14], based on the cross-Kerr nonlinearity which is generated in a five-level atomic medium. In a QPG, one qubit gets a phase conditional to the other qubit state according to the transformation [15, 16] $|i\rangle_1|j\rangle_2 \rightarrow \exp\{i\phi_{ij}\}|i\rangle_1|j\rangle_2$ where $\{i, j\} = 0, 1$ denote the logical qubit bases. This gate is universal when the conditional phase shift (CPS)

$$\phi = \phi_{11} + \phi_{00} - \phi_{10} - \phi_{01}, \quad (1)$$

is nonzero, and it is equivalent to a CNOT gate up to local unitary transformations when $\phi = \pi$ [15, 16]. Most of the literature focused only on the evaluation of the CPS and on the best conditions for achieving $\phi = \pi$ [10, 11, 12, 13, 14], while the gate fidelity, which is

the main quantity for estimating the efficiency of a gate, has been evaluated in the full quantum limit in Ref. [17] for the first time. Here we provide the details of the calculation of the fidelity and the CPS of Ref. [17], which showed the presence of a general *trade-off* between a large CPS and a gate fidelity close to one, hindering the QPG operation, in the stationary state. However, we shall see that this trade-off can be partially bypassed in the transient regime, which has never been considered before in EIT situations, still allowing a satisfactory gate performance.

The qubits are given by polarized single-photon wave packets with different frequencies, and the phase shifts ϕ_{ij} are generated when these two pulses cross an atomic ensemble in a five-level M configuration (see Fig. 1). The population is assumed to be initially in the ground state $|3\rangle$. From this ground state, it could be excited by either the single-photon *probe* field, with central frequency ω_p and coupling to transition $|3\rangle \leftrightarrow |2\rangle$, or by the single-photon *trigger* field, with central frequency ω_t and coupling to transition $|3\rangle \leftrightarrow |4\rangle$. We assume that the five levels are Zeeman sub-levels of an alkali atom, and that both pulses have a sufficiently narrow bandwidth. In this way, the Zeeman splittings can be chosen so that the atomic medium is coupled only to a given circular polarization of either the probe or trigger field, while it is transparent for the orthogonally polarized mode, which crosses the gas undisturbed [11]. As a consequence, the logical basis for each qubit practically coincides with the two lowest Fock states of the mode with the “right” polarization, $|0_j\rangle$ and $|1_j\rangle$ ($j = p, t$), while the “wrong” polarization modes will be neglected from now on.

A classical pump field, with frequency ω_1 and Rabi frequency Ω_1 , couples to the transition $|1\rangle \leftrightarrow |2\rangle$, while a second classical pump field, with frequency ω_4 and Rabi frequency Ω_4 , couples to the transition $|4\rangle \leftrightarrow |5\rangle$ (see Fig. 1). We consider a cylindrical, quasi-1D, atomic medium with the two classical pump beams propagating along its axis, collinear with the two quantum fields in order to avoid Doppler broadening. When the probe field is on two-photon resonance with the pump field with

*Electronic address: stojan.rebic@unicam.it

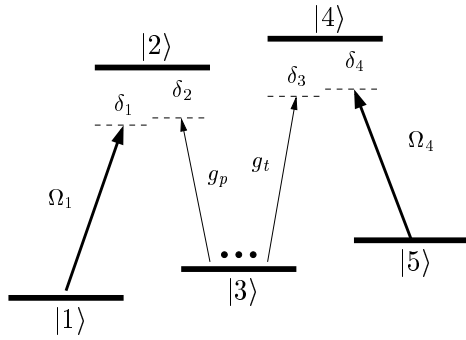


FIG. 1: Energy levels of the M -scheme. Ω_j are the Rabi frequencies of classical fields, while $g_{p,t}$ denote couplings of the quantized probe and trigger fields to their respective transitions. δ_j are the detuning of the fields from resonance.

Rabi frequency Ω_1 , and the trigger field is on two-photon resonance with the pump field with Rabi frequency Ω_4 , the system exhibits EIT for probe and trigger simultaneously. This simultaneous EIT condition is achieved when

$$\delta_1 = \delta_2, \quad \delta_3 = \delta_4, \quad (2)$$

where the detunings δ_j are defined by

$$E_2 - E_1 = \hbar\omega_1 + \hbar\delta_1, \quad (3a)$$

$$E_2 - E_3 = \hbar\omega_p + \hbar\delta_2, \quad (3b)$$

$$E_4 - E_3 = \hbar\omega_t + \hbar\delta_3, \quad (3c)$$

$$E_4 - E_5 = \hbar\omega_4 + \hbar\delta_4. \quad (3d)$$

A nonzero CPS occurs whenever a nonlinear cross-phase modulation (XPM) between probe and trigger is present. This cross-Kerr interaction takes place if the two-photon resonance condition is violated. For small frequency mismatch $\epsilon_{12} = \delta_1 - \delta_2$ and $\epsilon_{34} = \delta_3 - \delta_4$ (both chosen to be within the EIT window), absorption remains negligible and the cross-Kerr interaction between probe and trigger photons may be strong. The consequent CPS may become large, of the order of π , if the probe and trigger pulse interact for a sufficiently long time. If the two single photon pulses enter simultaneously the atomic medium, their interaction time t_{int} is optimized when the group velocities of the two pulses are equal, so that $t_{int} = L/v_g$, where v_g is the common group velocity of the pulses and L is the length of the gas cell. The inherent *symmetry* of the scheme guarantees perfect group velocity matching for probe and trigger whenever $\delta_1 = \delta_4$, $\delta_2 = \delta_3$ and $g_p/\Omega_1 = g_t/\Omega_4$, where $g_j = \mu_j \sqrt{\omega_j/2\hbar\epsilon_0} V_j$ ($j = p, t$) is the coupling constant between the quantum mode with frequency ω_j and mode volume V_j , and the corresponding transition with electric dipole moment μ_j .

The importance of group velocity matching for achieving a significant nonlinear phase shift was first pointed out in Ref. [10], which suggested to use a mixture of two different atomic species to achieve this goal. The first kind of atoms generates XPM by means of a four-level N

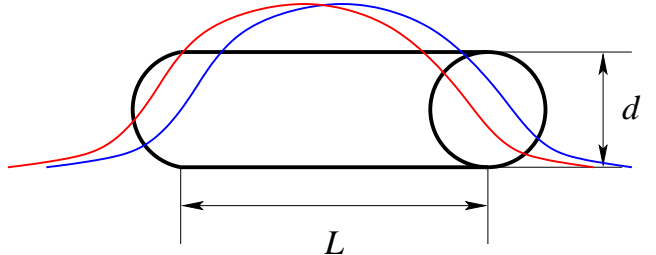


FIG. 2: A schematic plot of the assumed single-photon pulse propagation through the gas cell of length L and diameter d (color online). The pulse length is assumed to coincide with the cell length L , and the pulse waist w is assumed to be of order of cell diameter d .

scheme [6], in which however only the probe field undergoes EIT and it is slowed down, while the second kind of atoms realizes a three-level Λ scheme able to slow down the trigger pulse. Group velocity matching is achieved by means of an accurate but difficult control of the atomic densities. A different way of achieving group velocity matching, but which is still asymmetric for probe and trigger has been proposed in Ref. [11], which employs a five-level M scheme similar to the one discussed here, but with a different atomic population distribution. In that case, the two group velocities can be tuned and made equal simply by tuning the frequencies and intensities of the two classical pump fields. Instead, Ref. [12] considered a six level scheme in which probe and trigger are affected by EIT and XPM in a symmetric fashion, so that the corresponding group velocities are equal by construction. The present proposal achieves group velocity matching just in the same way (see also Refs. [13], where a four-level tripod system, symmetric between probe and trigger, has been proposed for XPM).

The paper is organized as follows. In Sec. II we describe the model used in the remainder of the paper. Sec. III shows the results of a perturbative calculation for the CPS. These are used as a motivation to pass to a density matrix based calculations in Sec. IV, describing a QPG operation in a steady-state. Then, the transient regime is explored in Sec. V, while in Sec. VI a scheme for the experimental verification of the QPG operation is discussed in detail. Conclusions are given in Sec. VII.

II. MODEL

In this Section, we present the model we have adopted for a full quantum description of the interaction of the two single-photon wave-packets with the atomic medium possessing the level structure outlined in Fig. 1. To this end, we make the following two assumptions which, even though not simple to realize experimentally, are more technical than physical in nature:

1. We assume perfect spatial mode matching between the input single-photon pulses entering the gas cell

and the optical modes naturally excited by the driven atomic medium, and which are determined by the geometrical configuration of the gas cell and of the pump beams [18]. This allows us to describe the probe and trigger fields with the right polarization in terms of *single* travelling optical modes, with annihilation operators $\hat{a}_{p,t}$.

2. We assume that the pulses are tailored in such a way that they simultaneously enter gas cell and completely overlap with it during the interaction (see Fig. 2). This means that their length (compressed inside a medium due to group velocity reduction) is of the order of the cell length L and their beam waist is of the order of the cell radius. In this way, the two pulses interact with *all* N_a atoms in the cell at once, and moreover, one can ignore spatial aspects of pulse propagation.

With these assumptions, and neglecting dipole-dipole interactions, the interaction picture Hamiltonian may be written as

$$\begin{aligned} H = & \hbar\epsilon_{12}\hat{S}_{11} + \hbar\delta_2\hat{S}_{22} + \hbar\delta_3\hat{S}_{44} + \hbar\epsilon_{34}\hat{S}_{55} \quad (4) \\ & + \hbar\Omega_1\sqrt{N_a}(\hat{S}_{21} + \hat{S}_{12}) + \hbar g_p\sqrt{N_a}(\hat{a}_p\hat{S}_{23} + \hat{S}_{32}\hat{a}_p^\dagger) \\ & + \hbar g_t\sqrt{N_a}(\hat{a}_t\hat{S}_{43} + \hat{S}_{34}\hat{a}_t^\dagger) + \hbar\Omega_4\sqrt{N_a}(\hat{S}_{45} + \hat{S}_{54}), \end{aligned}$$

where we have defined the collective atomic operators

$$\hat{S}_{kl} = \frac{1}{\sqrt{N_a}}\sum_{i=1}^{N_a}\sigma_{kl}^i, \quad k \neq l = 1, \dots, 5, \quad (5a)$$

$$\hat{S}_{kk} = \sum_i \sigma_{kk}^i, \quad (5b)$$

with $\sigma_{kl}^i \equiv |k\rangle_i\langle l|$ being the operator switching between states k and l of the i th atom. The initial state of the system corresponds to a probe and a trigger single-photon pulse with generic polarization, simultaneously entering the medium in which all the atoms are initially in state $|3\rangle$. Since we consider only the polarization mode interacting with the medium, both for the probe and the trigger, the initial state can be written as

$$\begin{aligned} |\psi_{in}\rangle = & \bigotimes_{i=1}^{N_a} |3\rangle_i \otimes (c_{00}|0_p\rangle \otimes |0_t\rangle + c_{01}|0_p\rangle \otimes |1_t\rangle \\ & + c_{10}|1_p\rangle \otimes |0_t\rangle + c_{11}|1_p\rangle \otimes |1_t\rangle). \quad (6) \end{aligned}$$

Due to the above assumptions, the passage of the two pulses through the atomic medium of length L corresponds to the time evolution of this state, for a time $t_{int} = L/v_g$, according to the master equation [5]

$$\begin{aligned} \dot{\rho} = & -\frac{i}{\hbar}[H, \rho] + \sum_k \frac{\gamma_{kk}}{2} \sum_{j=1}^{N_a} (2\sigma_{kk}^j \rho \sigma_{kk}^j - \sigma_{kk}^j \rho - \rho \sigma_{kk}^j), \\ & + \sum_{kl} \frac{\gamma_{kl}}{2} \sum_{j=1}^{N_a} (2\sigma_{kl}^j \rho \sigma_{kl}^{j\dagger} - \sigma_{kl}^{j\dagger} \sigma_{kl}^j \rho - \rho \sigma_{kl}^{j\dagger} \sigma_{kl}^j), \quad (7) \end{aligned}$$

including not only the coherent interaction described by the Hamiltonian of Eq. (4), but also the spontaneous emission from the excited states $l = 2, 4$ to the ground states $k = 1, 3, 5$ (γ_{kl} denotes the corresponding decay rate) and the dephasing of levels $|k\rangle$, $k = 1, 2, 4, 5$, with dephasing rate γ_{kk} . Typically the dephasing rates are much smaller than the decay rates, $\gamma_{kl} \gg \gamma_{kk}, \forall k, l$.

Since the initial state of Eq. (6) contains at most two excitations, the coherent time evolution driven by Eq. (4) is simple and restricted to a finite-dimensional Hilbert space involving few symmetric collective atomic states. In fact, each component of the initial state of Eq. (6) evolves independently in a different subspace. The component with no photon is an eigenstate of H and does not evolve. The $\bigotimes_{i=1}^{N_a} |3\rangle_i |0_p\rangle \otimes |1_t\rangle$ component evolves in a three-dimensional Hilbert space which it spans together with the two states $|e_4^{(0,0)}\rangle$ and $|e_5^{(0,0)}\rangle$. Here, we have defined the symmetric collective states

$$|e_r^{(n_p, n_t)}\rangle = \frac{1}{\sqrt{N_a}} \sum_{i=1}^{N_a} |3_1, 3_2, \dots, r_i, \dots, 3_{N_a}\rangle \otimes |n_p\rangle \otimes |n_t\rangle, \quad (8)$$

where $r = 1, 2, 4, 5$. In a similar fashion, the component with only one probe photon evolves in a three-dimensional Hilbert space spanned by the three states $\bigotimes_{i=1}^{N_a} |3\rangle_i |1_p\rangle \otimes |0_t\rangle$, $|e_1^{(0,0)}\rangle$ and $|e_2^{(0,0)}\rangle$. The component with one probe and one trigger photon evolves in the five dimensional subspace spanned by the four collective states $|e_1^{(0,1)}\rangle$, $|e_2^{(0,1)}\rangle$, $|e_4^{(1,0)}\rangle$, and $|e_5^{(1,0)}\rangle$ and the state $\bigotimes_{i=1}^{N_a} |3\rangle_i |1_p\rangle \otimes |1_t\rangle$.

Decoherence effects, and more specifically spontaneous emission from each atom complicates this dynamics. However, we are in the weak excitation limit where, for $l \neq 3$, $\langle\sigma_{ll}^j\rangle \simeq N_a^{-1} \ll 1$, as shown by the fact that the Hamiltonian dynamics involve only the symmetric atomic states of the form of Eq. (8). This limit allows a drastic simplification of the effective time evolution. Following Duan *et al.* [19], we can introduce Fourier transforms of the individual atomic operators $s_{kl}^\mu = \sum_{j=0}^{N_a-1} \sigma_{kl}^j e^{ij\mu/N_a} / \sqrt{N_a}$, where $s_{kl}^0 = \hat{S}_{kl}$ are the collective operators defined in Eq. (5a). The sum over the atoms in Eq. (7) then transforms to the sum over the collective atomic modes with index μ . In the weak excitation limit, the operators s_{kl}^μ approximately commute with each other. This means that they represent independent collective atomic modes, and one can trace over the $\mu \neq 0$ modes, so that the spontaneous emission term in the master equation becomes

$$\sum_{kl} \frac{\gamma_{kl}}{2} (2\hat{S}_{kl}\rho\hat{S}_{kl}^\dagger - \hat{S}_{kl}^\dagger\hat{S}_{kl}\rho - \rho\hat{S}_{kl}^\dagger\hat{S}_{kl}), \quad (9)$$

where the sum is now over the six “collective” spontaneous decay channels only, each characterized by the *single-atom* decay rate γ_{kl} . A similar argument applies to the dephasing term in the master equation (7). In fact, if we restrict to the subspace of the symmetric collective

states of Eq. (8) involving only single atomic excitations, we can approximate in the dephasing terms of the master equation,

$$\sum_k \gamma_{kk} \sum_{j=1}^{N_a} \sigma_{kk}^j \rho \sigma_{kk}^j \simeq \sum_k \gamma_{kk} \hat{S}_{kk} \rho \hat{S}_{kk}, \quad (10)$$

where \hat{S}_{kk} is given by Eq. (5b). Using Eqs. (9) and (10), the master equation of Eq. (7) in the weak excitation limit becomes

$$\begin{aligned} \dot{\rho} = & -\frac{i}{\hbar} [H, \rho] + \sum_k \frac{\gamma_{kk}}{2} \left(2\hat{S}_{kk} \rho \hat{S}_{kk} - \hat{S}_{kk} \rho - \rho \hat{S}_{kk} \right) \\ & + \sum_{kl} \frac{\gamma_{kl}}{2} \left(2\hat{S}_{kl} \rho \hat{S}_{kl}^\dagger - \hat{S}_{kl}^\dagger \hat{S}_{kl} \rho - \rho \hat{S}_{kl}^\dagger \hat{S}_{kl} \right), \end{aligned} \quad (11)$$

that is, it involves only the operators of the collective atomic mode with index $\mu = 0$. This actually means that the single photon probe and trigger pulses excite only a restricted number of collective atomic states, so that the atomic medium behaves as an effective *single* 5-level atom, with a *collectively enhanced* coupling with the optical modes $g_j \sqrt{N_a}$, but with single-atom decay rates γ_{kl} , dephasing rates γ_{kk} , Rabi frequencies Ω_i , and detunings δ_i .

Spontaneous emission causes the four independent Hilbert subspaces corresponding to the four initial state components to become coupled. Moreover, the “cross” decay channels $|4\rangle \rightarrow |1\rangle$ and $|2\rangle \rightarrow |5\rangle$ couple the above-mentioned collective states with six new states, $|e_1^{(1,0)}\rangle$, $|e_2^{(1,0)}\rangle$, $|e_3^{(2,0)}\rangle$ (populated if $\gamma_{41} \neq 0$), and $|e_5^{(0,1)}\rangle$, $|e_4^{(0,1)}\rangle$, $|e_3^{(0,2)}\rangle$ (populated if $\gamma_{25} \neq 0$). Therefore Eq. (11) actually describes dynamics in a Hilbert space of dimension 18, which we have numerically solved in order to establish the performance of the QPG. Notice that, due to the combined action of the cross-decay channels and of the Hamiltonian (4), the states $|e_1^{(1,0)}\rangle$, $|e_2^{(1,0)}\rangle$, $|e_5^{(0,1)}\rangle$ and $|e_4^{(0,1)}\rangle$ are coupled also to *doubly excited* atomic collective states without photons which are neglected by our treatment. However, as we shall see below in the paper, a good QPG performance is possible only when spontaneous emission events are rare. Under this condition, the probability to populate these doubly excited atomic collective states during the atom-field interaction is completely negligible, and therefore our model based on the effective single five-level atom description provided by Eq. (11) is essentially correct.

In summary, the model outlined above relies on the single-photon nature of the excitations. In this case, the collective operators (5) effectively switch between the states making the superposition $|\psi_{in}\rangle$ (6), and the symmetric collective states $|e_r^{(n_p, n_t)}\rangle$ (8). This is central to the reasoning leading to the effective master equation (11).

To characterize the QPG operation, we calculate the CPS ϕ of Eq. (1) and the *fidelity* of the gate. The accumulated CPS ϕ as a function of the interaction time t_{int}

is obtained by using the fact that the phase shifts ϕ_{ij} of Eq. (1) are given by combinations of the phases of the off-diagonal matrix elements (in the Fock basis) of the reduced density matrix of the probe and trigger modes, $\rho_f(t) = \text{Tr}_{atoms}\{\rho(t)\}$.

The gate fidelity is given by [16]

$$\mathcal{F}(t) = \sqrt{\langle \psi_{id}(t) | \rho_f(t) | \psi_{id}(t) \rangle}, \quad (12)$$

where

$$\begin{aligned} |\psi_{id}(t)\rangle = & c_{00} \exp\{i\phi_{00}(t_{int})\} |0_p, 0_t\rangle \\ & + c_{01} \exp\{i\phi_{01}(t)\} |0_p, 1_t\rangle \\ & + c_{10} \exp\{i\phi_{10}(t)\} |1_p, 0_t\rangle \\ & + c_{11} \exp\{i\phi_{11}(t)\} |1_p, 1_t\rangle \end{aligned} \quad (13)$$

is the ideally evolved state from the initial condition (6), with phases $\phi_{ij}(t)$ evaluated from $\rho_f(t)$ as discussed above. The overbar denotes the average over all initial states (i.e., over the c_{ij} , see Poyatos *et al.* [20]). The above fidelity characterizes the performance of the QPG as a deterministic gate. However, one could also consider the QPG as a *probabilistic* gate, whose operation is considered only when the number of output photons is equal to the number of input photons. The performance of this probabilistic QPG could be experimentally studied by performing a conditional detection of the phase shifts, and it is characterized by the *conditional* fidelity $\mathcal{F}^c(t)$, which will be discussed in Sec. IV.

III. PERTURBATIVE REGIME

The conditional fidelity is always larger than the unconditional one, but they become equal (and both approach 1) for an ideal QPG in which the number of photons is conserved and all the atoms remain in state $|3\rangle$. This ideal condition is verified in the limit of large detunings $\delta_j \gg \gamma_{kj}$ so that spontaneous emission is significantly suppressed and can be neglected, and very small couplings $g_j \sqrt{N_a} \ll \Omega_j$. In this limit, each component of the initial state of Eq. (6) practically coincides with the dark state of the four independent Hamiltonian dynamics discussed in Sec. II. The system with the initial state containing zero probe and trigger photons does not evolve, i.e. stays in the initial state $\bigotimes_{i=1}^{N_a} |3\rangle_i |0_p\rangle \otimes |0_t\rangle$ all the time. The subsystem containing one probe and zero trigger photons as the initial state evolves according to a reduced three-dimensional Hamiltonian, which in the basis formed by the states $\bigotimes_{i=1}^{N_a} |3\rangle_i |1_p\rangle \otimes |0_t\rangle$, $|e_2^{(0,0)}\rangle$ and $|e_1^{(0,0)}\rangle$, is given by

$$H_p = \begin{pmatrix} 0 & g_p \sqrt{N_a} & 0 \\ g_p \sqrt{N_a} & \delta_2 & \Omega_1 \\ 0 & \Omega_1 & \epsilon_{12} \end{pmatrix}. \quad (14a)$$

Similarly, the subsystem containing one trigger and zero probe photons as the initial state evolves according to

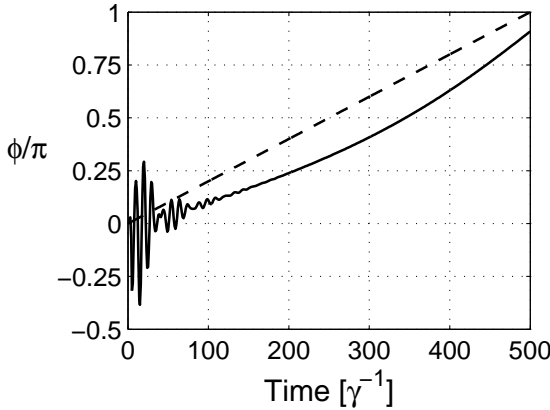


FIG. 3: Conditional phase shift as a function of the interaction time for $N_a = 10^6$, $\delta_1 = \delta_3 = 7.5\gamma$, $\epsilon_{12} = \epsilon_{34} = 0.05\gamma$, $g_p = g_t = 0.0011\gamma$, $\Omega_1 = \Omega_4 = 1.875\gamma$ and $\gamma_{kk} = \gamma_{ph} = 10^{-3}\gamma$, $\forall k$. We have taken equal decay rates, $\gamma_{21} = \gamma_{23} = \gamma_{25} = \gamma_{41} = \gamma_{43} = \gamma_{45} = \gamma/3$, with $\gamma = 2\pi \times 6$ MHz. Solid line represents the phase shift, as calculated from the full master equation, while the dashed line gives the perturbative prediction of Eq. (16).

a reduced three-dimensional Hamiltonian, which in the basis formed by the states $\bigotimes_{i=1}^{N_a} |3\rangle_i |0_p\rangle \otimes |1_t\rangle$, $|e_4^{(0,0)}\rangle$ and $|e_5^{(0,0)}\rangle$, is given by

$$H_t = \begin{pmatrix} 0 & g_t\sqrt{N_a} & 0 \\ g_t\sqrt{N_a} & \delta_3 & \Omega_4 \\ 0 & \Omega_4 & \epsilon_{34} \end{pmatrix}. \quad (14b)$$

Finally, the subsystem containing initially one photon each in probe and trigger modes evolves according to a reduced five-dimensional Hamiltonian, which in the basis formed by the states $|e_1^{(0,1)}\rangle$, $|e_2^{(0,1)}\rangle$, $\bigotimes_{i=1}^{N_a} |3\rangle_i |1_p\rangle \otimes |1_t\rangle$, $|e_4^{(1,0)}\rangle$, and $|e_5^{(1,0)}\rangle$, is given by

$$H_{pt} = \begin{pmatrix} \delta_2 & \Omega_1 & g_p\sqrt{N_a} & 0 & 0 \\ \Omega_1 & \epsilon_{12} & 0 & 0 & 0 \\ g_p\sqrt{N_a} & 0 & 0 & g_t\sqrt{N_a} & 0 \\ 0 & 0 & 0 & \delta_3 & \Omega_4 \\ 0 & 0 & g_t\sqrt{N_a} & \Omega_4 & \epsilon_{34} \end{pmatrix}. \quad (14c)$$

The phase accumulation experienced by the various components of the quantum state of the fields will be proportional to the eigenvalues of these matrices. The four phase shifts ϕ_{ij} can be evaluated as a fourth-order perturbation expansion of the eigenvalue corresponding to the dark state in each subspace, multiplied by the interaction time t_{int} . The CPS is then calculated as

$$\phi = (\lambda_{H_{pt}} - \lambda_{H_p} - \lambda_{H_t})t_{int}, \quad (15)$$

where the λ 's denote the eigenvalues of the corresponding reduced Hamiltonian, with $\lambda_{H_{pt}} \leftrightarrow \phi_{11}$, $\lambda_{H_p} \leftrightarrow \phi_{10}$, $\lambda_{H_t} \leftrightarrow \phi_{01}$ and $\phi_{00} = 0$, in agreement with the general definition of Eq. (1). Following this procedure results in

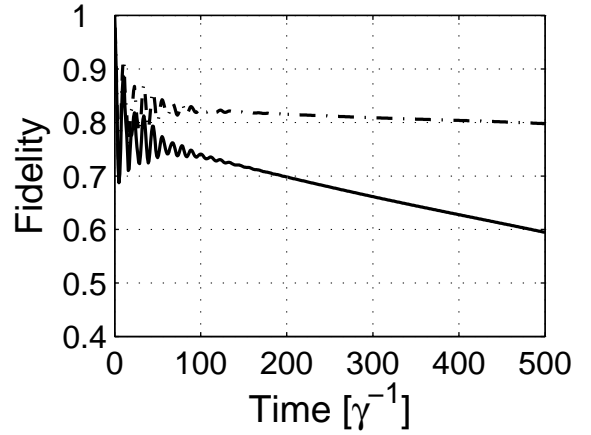


FIG. 4: Gate fidelity of Eq. (12) versus the interaction time, for the same set of parameters as in Fig. 3. The solid line is the unconditional gate fidelity $\mathcal{F}(t)$, while the dot-dashed line is the conditional one, $\mathcal{F}^c(t)$.

the following CPS

$$\phi = \frac{g_p^2 g_t^2 N_a^2 t_{int}}{(\epsilon_{34}\delta_3 - \Omega_4^2)(\epsilon_{12}\delta_2 - \Omega_1^2)} \times \left[\frac{\epsilon_{34}(\epsilon_{12}^2 + \Omega_1^2)}{(\epsilon_{12}\delta_2 - \Omega_1^2)} + \frac{\epsilon_{12}(\epsilon_{34}^2 + \Omega_4^2)}{(\epsilon_{34}\delta_3 - \Omega_4^2)} \right]. \quad (16)$$

This prediction is verified by the numerical solution of Eq. (11) in the limit of large detunings and small couplings. However the resulting CPS is too small, even for very long interaction times (i.e., long gas cells): for example, for $g_p, t\sqrt{N_a} = 0.5$ MHz, $\epsilon_{12,34} = 1.9$ MHz, $\Omega_{1,4} = 65$ MHz and $\delta_{2,3} = 1.9$ GHz, we obtain a tiny CPS of only 3×10^{-4} radians when $t_{int} = 10^{-4}$ s, which corresponds to $L \simeq 30$ Km. This is not surprising because this limit corresponds to a dispersive regime far from EIT. In this regime, transparency is achieved by means of a strong coupling field, producing a well-separated Autler-Townes doublet [5]. At the same time, the size of nonlinearity is small due to the extremely weak coupling of the quantized fields to their respective transitions. The results are, therefore, not different from those expected from XPM in a standard optical fiber. Therefore, one has to explore the non-perturbative regime of larger couplings in order to exploit the low-noise, large-nonlinearity properties of EIT and achieve a satisfactory QPG operation.

IV. STEADY-STATE QPG OPERATION

A large amount of work exploring EIT-based nonlinear optical phenomena considers the steady-state of a generic EIT-based system as being the natural state in which to predict and test different phenomena [6, 7, 9, 11]. We shall see in this Section that it is not possible to achieve a satisfactory QPG performance in such a steady-state regime.

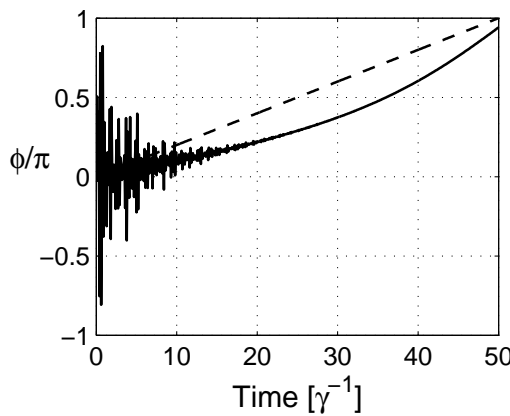


FIG. 5: Conditional phase shift as a function of the interaction time for $N_a = 10^6$, $\delta_1 = \delta_3 = 9.5\gamma$, $\epsilon_{12} = \epsilon_{34} = 0.2\gamma$, $g_p = g_t = 0.018\gamma$ and $\Omega_1 = \Omega_4 = 19\gamma$ and $\gamma_{kk} = \gamma_{ph} = 10^{-3}\gamma$, $\forall k$. We have taken equal decay rates, $\gamma_{21} = \gamma_{23} = \gamma_{25} = \gamma_{41} = \gamma_{43} = \gamma_{45} = \gamma/3$, with $\gamma = 2\pi \times 6$ MHz. Solid line represents the phase shift, as calculated from a density matrix, while the dashed line gives the eigenvalue solution.

In this Section, we analyze the performance of the QPG at the steady state. To this end, we consider two different parameter regimes: (i) the regime of long interaction times, a natural extension of the perturbation analysis of Sec. III, and (ii) the regime of short interaction times, corresponding to a non-perturbative regime with strong atom-field coupling.

A. Long Interaction Time

Naturally extending the perturbative analysis, we solve the master equation (11), and show the results in Figs. 3 and 4. Fig. 3 shows the result for the conditional phase shift. Solid line has been calculated from the solution of Eq. (11), as explained in Sec. II. The dashed line is the ‘benchmark’ solution, obtained from the eigenvalues of the associated Hamiltonian, by using Eq. (15). The eigenvalues of the Hamiltonians of Eqs. (14) have been calculated numerically for the set of parameters of Fig. 3.

It is evident that the ‘benchmark’ solutions offers a reasonably good estimate for the size of the CPS. The exact dynamics driven by the master equation (11) presents an additional oscillatory behavior both on a short time scale (transient processes), and on a long-time scale. The longer time scale comes from the fact that to induce the cross-Kerr nonlinearity, one has to detune the fields away from the dark resonance. This detuning is very small and is seen in the oscillations on a long time-scale. As both probe and trigger fields are detuned by the same amount, only one frequency of long-time oscillations is observed.

In Fig. 4, fidelities (averaged over all possible two-qubit initial states) are shown in two cases. Both are calculated by using Eq. (12), but they differ in the way $\rho_f(t)$ is defined. The solid line in Fig. 4 refers to the *unconditional*

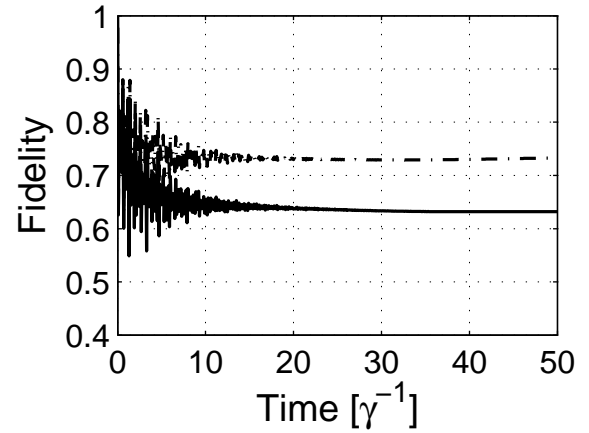


FIG. 6: Fidelity, averaged over the initial states of a two-qubit system, for the same set of parameters as in Fig. 5. Solid line is the unconditional gate fidelity, while dot-dashed line is the conditional one.

fidelity $\mathcal{F}(t)$, which is calculated from Eq. (12) by taking $\rho_f(t) = \text{Tr}_{at}\{\rho(t)\}$, where $\rho(t)$ is the solution of the master equation (11). The unconditional fidelity quantifies the performance of the QPG as a *deterministic* gate for single-photon qubits.

The dot-dashed line in Fig. 4 refers to the *conditional* fidelity $\mathcal{F}^c(t)$, which is evaluated according to Eq. (12), but with $\rho_f(t)$ replaced by $\rho_f^c(t) = \text{Tr}_{at}\{|\psi_{nj}(t)\rangle\langle\psi_{nj}(t)|\}/\langle\psi_{nj}(t)|\psi_{nj}(t)\rangle$, where $|\psi_{nj}(t)\rangle$ is the (non-normalized) evolved atom-field state conditioned to the detection of no quantum jumps [22], i.e., of no photon loss by spontaneous emission. This fidelity can be measured by post-selecting those measurement results that conserve photon number, i.e., discarding those data sets where at least a photon from the initial two-qubit state has been lost to the environment. The conditional fidelity quantifies the performance of the QPG as a *probabilistic* two-qubit gate.

In Figs. 3 and 4, we have found at best a CPS of $\sim \pi$ in correspondence with fidelities $\mathcal{F}(t_{int})$ and $\mathcal{F}^c(t_{int})$ equal to 60% and 80%, respectively. This is due to the general presence of a *trade-off between the size of the CPS and of the gate fidelity*, as well as to the atomic dephasing [27]. This is an important result of our paper, which actually holds true in *any* EIT-based nonlinear optics systems. In fact, both the conditional and the unconditional gate fidelity approach 1 in the limit of very small g_j , but this limit yields a CPS which becomes appreciable only for unrealistically long gas cells. Therefore a larger CPS requires a larger ratio $g_j\sqrt{N_a}/\Omega_j$. This condition however increases the population of the collective atomic states $|e_1^{(n_p, n_t)}\rangle$ and $|e_5^{(n_p, n_t)}\rangle$ at the expense of the initial atomic state $|3\rangle$, thus unavoidably decreasing the gate fidelity. Similar conclusions hold for other options, such as increased detunings δ_j , or adjusting two-photon detunings ϵ_{ij} . Therefore, just the pure coherent unitary evolution of the system, governed by the Hamiltonian of

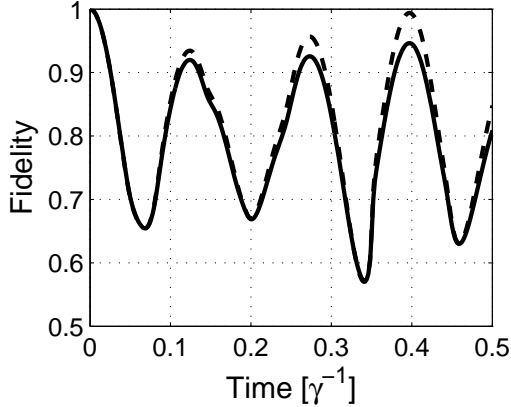


FIG. 7: Fidelity of the QPG operation for $N_a = 10^6$, $\delta_1 = \delta_3 = 15\gamma$, $\epsilon_{12} = \epsilon_{34} = 0.01\gamma$, $g_p = g_t = 0.0022\gamma$, $\Omega_1 = \Omega_4 = 4\gamma$ and $\gamma_{kk} = \gamma_{ph} = 10^{-3}\gamma$, $\forall k$. We have taken equal decay rates, $\gamma_{21} = \gamma_{23} = \gamma_{25} = \gamma_{41} = \gamma_{43} = \gamma_{45} = \gamma/3$, with $\gamma = 2\pi \times 6$ MHz. The unconditional fidelity (solid) and conditional fidelity (dashed) are shown. See text for details.

Eq. (4) causes this inherent trade-off.

B. Short Interaction Time

To further illustrate our findings, we calculate the CPS and the gate fidelities in the range of parameters where the total interaction time is an order of magnitude smaller than in Sec. IV A. The CPS and the gate fidelities are calculated as described in Sec. IV A, and the results are shown in Figs. 5 and 6. To obtain a CPS of the order of π in a shorter interaction time ($t_{int} \sim 50/\gamma$), we have assumed a larger ratio $g_j\sqrt{N_a}/\Omega_j$. The trade-off between the amount of accumulated nonlinear phase shift and the gate fidelity is now even more pronounced: we find at best a CPS of $\sim \pi$ in correspondence with fidelities $\mathcal{F}(t_{int})$ and $\mathcal{F}^c(t_{int})$ equal to 65% and 73%, respectively. As expected, having a stronger atom-field coupling enhances the processes lowering the fidelity. The system ends up with a large CPS faster, but this is achieved with a final state in which the probability of loosing the probe and trigger photons by spontaneous emission or within the atomic medium is no more negligible. We notice that in this short interaction time case dephasing does not have an appreciable effect, that is, the results without dephasing are indistinguishable from those with dephasing shown in Figs. 5 and 6, due to fact that dephasing rates in a dilute gas are typically much smaller than decay rates. The only possible way to circumvent this trade-off is to explore the transient regime, which will be discussed in the following Section.

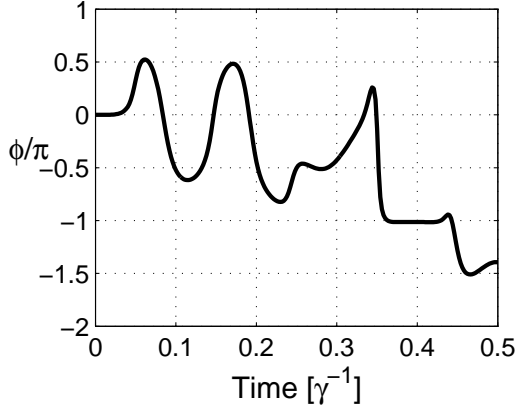


FIG. 8: Conditional phase shift ϕ versus the interaction time, for the parameters of Fig. 7. See text for details.

V. QPG OPERATION IN TRANSIENT REGIME

In Sec. IV, we have found that the QPG operation of EIT-based nonlinear system in a steady-state is plagued by the trade-off between the phase shift size and the gate fidelity. In an attempt to find favorable conditions for the QPG operation, we consider the transient regime, when $\gamma t_{int} \lesssim 1$. As discussed above, in order to accumulate a significant CPS in such a short time one has to consider the strong coupling regime with a large ratio $g_j\sqrt{N_a}/\Omega_j$. Therefore, the trade-off between fidelity and a large nonlinear interaction is present also in the transient regime. However, when $g_j\sqrt{N_a}/\Omega_j$ is large, the transient dynamics is characterized by Rabi-like oscillations of the atomic populations and of the photon number, determining, as a consequence, coherent oscillations of the gate fidelity. In such a case one cannot exclude the existence of special values of the interaction time t_{int} corresponding to a maximum of the gate fidelity close to one, and at the same time, to a value of the CPS close to π .

We show that this fact is actually possible in Figs. 7 and 8, where we see that a CPS of $\sim \pi$ radians is obtained in the transient regime for $t_{int} \approx 0.4/\gamma \sim 10$ ns. At the same interaction time, the unconditional gate fidelity (Fig. 7, full line) is about 94%, while the conditional gate fidelity reaches the value of 99% (Fig. 7, dashed line). The conditional gate fidelity is obtained in correspondence with a success probability of the gate equal to 0.94, calculated from the norm of the Monte-Carlo wave function [22]. The probe and trigger group velocities are calculated to be $v_g \simeq 3 \times 10^6$ ms $^{-1}$, yielding a gas cell length $L = v_g t_{int} \simeq 3.1$ cm. The value of g_j yields an interaction volume $V \simeq 2 \cdot 10^{-3}$ cm 3 , corresponding to a gas cell diameter of about 330 μ m and to an atomic density $N_a/V \simeq 5 \cdot 10^{10}$ cm $^{-3}$.

To give a further example and to deepen our discussion of QPG performance and the CPS-fidelity trade-off, we now show the optimal results for the experimentally available pulses produced in the experiment of Darquié *et*

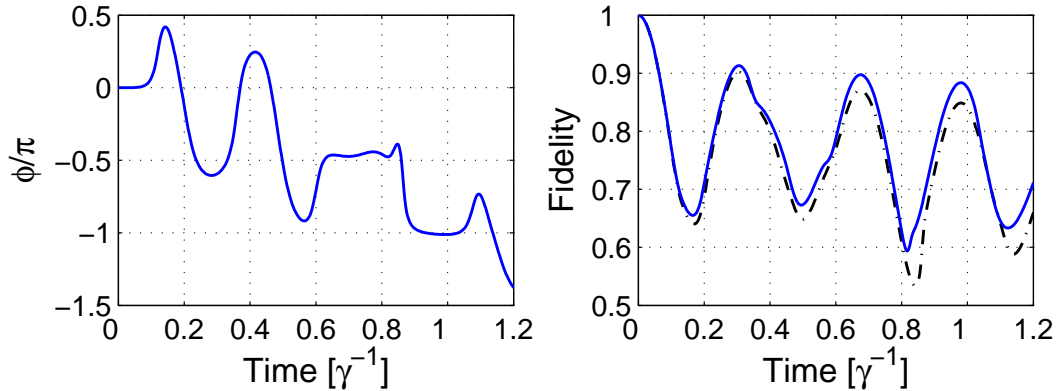


FIG. 9: Conditional phase shift (*left*) and the fidelity (*right*) of a QPG operation for $N_a = 10^8$, $\delta_2 = \delta_3 = 6\gamma$, $\epsilon_{12} = \epsilon_{34} = 0.05\gamma$, $g_p = g_t = 0.0009\gamma$ and $\Omega_1 = \Omega_4 = \gamma$. We have taken equal decay rates, $\gamma_{21} = \gamma_{23} = \gamma_{25} = \gamma_{41} = \gamma_{43} = \gamma_{45} = \gamma/3$. For ^{87}Rb , $\gamma = 2\pi \times 6$ MHz, giving the interaction time (i.e. pulse length) of $\simeq 25$ ns for $|\phi| \simeq \pi$. Dot-dashed line denotes the deterministic fidelity, while solid line denotes the conditional fidelity.

al. [21] (see Fig. 9). The length of a pulse produced in [21] is 26 ns ($\simeq \gamma^{-1}$). The optimal parameters of Fig. 9 give the unconditional gate fidelity (Fig. 9 *right*, dot-dashed line) of 85%, while the conditional fidelity reaches 89% (Fig. 9 *right*, solid line). The probe and trigger group velocities are calculated to be $v_g \simeq 1.51 \times 10^6$ ms $^{-1}$, yielding a gas cell length $L = v_g t_{int} \simeq 3.82$ cm. The value of g_j yields an interaction volume $V \simeq 10^{-1}$ cm 3 , corresponding to a gas cell diameter of about 910 μm and to an atomic density $N_a/V \simeq 10^9$ cm $^{-3}$. So, taking the longer wavepackets (i.e. longer interaction times) means that the CPS-fidelity trade-off becomes increasingly important, and the top value of fidelity decreases slightly with respect to its optimal value.

Note how in both cases (Figs. 7 and 9) high values of fidelity could be obtained for values of CPS lower than π radians. This implies the possibility of the implementation of a *universal* quantum gate [15], which requires only $\phi \neq 0$.

A comment about this calculation of the common group velocity of the two wave-packets, v_g , is in order. As mentioned earlier, EIT is stationary phenomenon, and in fact, the conventional v_g is a steady-state quantity which it is obtained from the susceptibility χ according to

$$v_g = c \left[1 + \frac{1}{2} \text{Re}[\chi] + \frac{\omega_0}{2} \left(\frac{\partial \text{Re}[\chi]}{\partial \omega} \right)_{\omega_0} \right]^{-1} \quad (17)$$

(ω_0 is the central frequency of wave-packet), where the susceptibility of the j -th field, χ_j ($j = p, t$), is evaluated from the associated steady-state atomic coherence ρ_j^{ss} as

$$\chi_j = \frac{N|\mu_j|^2}{V\hbar\varepsilon_0\Omega_j} \rho_j^{ss}. \quad (18)$$

Instead, the above results are obtained in the transient regime where $\gamma t_{int} < 1$, and for this reason we have estimated the group velocity in a different way. We

have evaluated the relevant time-dependent atomic coherence $\rho_j(t)$ and the corresponding “instantaneous susceptibility” $\chi_j(t)$ from the reduced atomic density matrix $\rho_{red}(t) = \text{Tr}_{fields}\{\rho(t)\}$, with $\rho(t)$ being the solution of Eq. (11). The corresponding “instantaneous” group velocity $v_g(t)$ has been then averaged over the time interval between 0 and t_{int} , providing in this way our estimate of the “transient” non-stationary group velocity of the single-photon wave-packets. For the parameters of Fig. 9, this non-stationary v_g is approximately equal to $c/100$ and it is about one order of magnitude smaller than the conventional v_g obtained from the steady-state susceptibility. This appreciable slowing down of the group velocity is a signature of a sort of “non-stationary” EIT process.

In order to verify that the non-stationary dynamics is really reminiscent of EIT, in the next subsection we compare these results with a numerical study of the three-level ladder atomic scheme (see Fig. 10), yielding XPM without EIT. Here we anticipate that we have found a smaller gate fidelity ($\sim 78\%$) for a corresponding set of parameters, providing therefore further support to the presence of a moderate, non-stationary EIT process in the transient dynamics of our five-level M scheme.

A. The Conventional Three-Level Scheme

The atomic ladder scheme (see Fig. 10) is well-known to exhibit XPM of the two fields involved [6]. In order to achieve a reasonable size of cross-phase shift, the detuning of the intermediate state δ_p needs to be large. This minimizes spontaneous emission ($\sim \gamma_2/\delta_p^2$), but also the size of XPM $\sim 1/\delta_p^2$.

In order to evaluate the XPM in a manner comparable to what we have done for the M -scheme, we make similar assumptions and arrive at a description analogous to the one described in Sec. II. The Hamiltonian is now given

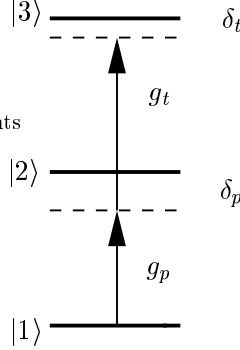


FIG. 10: Energy levels of the ladder scheme. $g_{p,t}$ denote couplings of the quantized probe and trigger fields to their respective transitions. $\delta_{p,t}$ are detunings of the probe and trigger fields from resonance.

by

$$H_3 = \hbar\delta_p\hat{S}_{22} + \hbar(\delta_p - \delta_t)\hat{S}_{33} + \hbar g_p \sqrt{N_a} (\hat{a}_p \hat{S}_{21} + \hat{S}_{12} \hat{a}_p^\dagger) + \hbar g_t \sqrt{N_a} (\hat{a}_t \hat{S}_{23} + \hat{S}_{23} \hat{a}_t^\dagger). \quad (19)$$

Following the same reasoning as in Sec. II, we arrive at the effective master equation (we neglect here atomic dephasing)

$$\begin{aligned} \dot{\rho} = \mathcal{L}_3 \rho = & -\frac{i}{\hbar} [H_3, \rho] \\ & + \frac{\gamma_{21}}{2} (2\hat{S}_{12}\rho\hat{S}_{21} - \hat{S}_{21}\hat{S}_{12}\rho - \rho\hat{S}_{21}\hat{S}_{12}) \\ & + \frac{\gamma_{32}}{2} (2\hat{S}_{23}\rho\hat{S}_{32} - \hat{S}_{23}\hat{S}_{32}\rho - \rho\hat{S}_{23}\hat{S}_{32}), \end{aligned} \quad (20)$$

where γ_{12} and γ_{23} denote the spontaneous emission rates from levels $|2\rangle$ and $|3\rangle$ to levels $|1\rangle$ and $|2\rangle$ respectively, and the operators \hat{S}_{ij} denote collective atomic operators, in the spirit of Eq. (5a).

The results of the calculation of unconditional quantities are shown in Fig. 11, for a parameter regime comparable to that discussed in relation to Figs. 8 and 8 (see also Ref. [17]) for the five-level M scheme. The atoms are assumed to be in the collective state $\bigotimes_{i=1}^{N_a} |2\rangle_i$ initially, as this is found to give better results. The reason is a more efficient photon-photon interaction since the initial state is symmetric with respect to probe and trigger photons. At the interaction time $t_{int} \approx 0.12/\gamma$, the CPS reaches the value $\sim \pi$ and at the same time the unconditional fidelity is found to be $\sim 78\%$. It is possible to see that the conditional fidelity, even though higher, always remains significantly lower than that obtained in the M -scheme.

Therefore, we conclude that the optimal results for the QPG operation can be found in the “transient EIT-regime”. The general trade-off between the nonlinear phase shift and the fidelity is still present, but it is compensated by the transient oscillations in the populations of atomic levels. In fact, the numerical results show that, in the parameter regime under consideration, the population of the excited states $|e_2^{(n_p, n_t)}\rangle$ and $|e_4^{(n_p, n_t)}\rangle$ is always

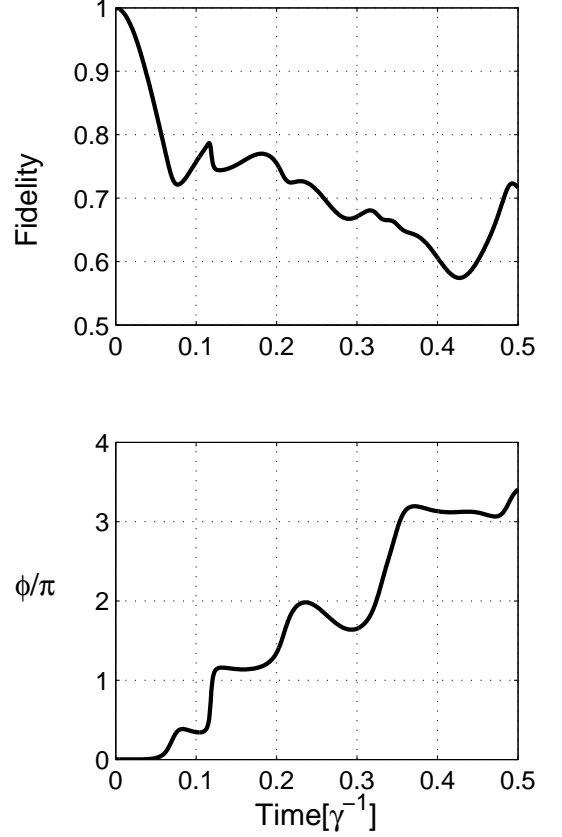


FIG. 11: Average fidelity (top figure) and conditional phase shift (bottom figure) as a function of time for the three-level ladder scheme of Fig. 10 and for $N_a = 10^8$, $\delta_p = 10\gamma$, $\delta_t = 0$ and $g_p = g_t = 0.0022\gamma$. The spontaneous emission rate is $\gamma_{21} = \gamma_{32} = \gamma = 2\pi \times 6$ MHz.

negligible, and one has coherent oscillations of the population between the states $|e_1^{(n_p, n_t)}\rangle$, $\bigotimes_i |3\rangle_i \otimes |n_p, n_t\rangle$ and $|e_5^{(n_p, n_t)}\rangle$. At the interaction time t_{int} corresponding to the maxima of the gate fidelity in Fig. 9, atoms are largely found in state $\bigotimes_i |3\rangle_i \otimes |n_p, n_t\rangle$, and the relative populations and phase relations between the states of the two photonic qubits are consistent with the “ideal” state of Eq. (13).

VI. EXPERIMENTAL VERIFICATION OF THE QPG OPERATION

In this Section, two possible schemes for experimental implementation are discussed. First is the detection in the occupation number logical basis, and the second is the detection in the polarization logical basis. The two bases are identical from the point of view of theoretical treatment, however, their implementation is different in practice.

Occupation number logical basis – In this section we describe a Michelson-like interferometer (see Fig 12) for

two-photons product state $|1_R\rangle|1_B\rangle$ with the ‘right’ σ^- circular polarization, where R (red) refers to the probe field and B (blue) to the trigger. We show that the interferometer is able to reveal and measure the QPG phase shift. The probe and trigger fields with a bandwidth of $40 \div 100$ MHz (corresponding to $25 \div 10$ ns 1/e half width pulse duration [21]) are separated in frequency by ~ 7 THz and are resonant with the ^{87}Rb hyperfine transitions $D_1F = 2 \rightarrow F' = 1$ at 794.7 nm (377.228 THz), and $D_2F = 2 \rightarrow F' = 1$ at 780.2 nm (384.225 THz), respectively.

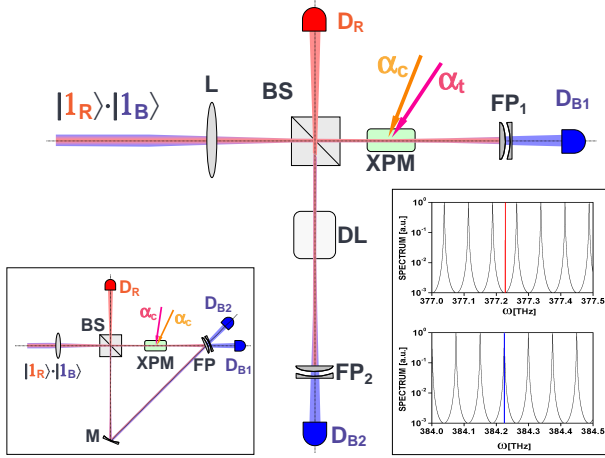


FIG. 12: Scheme of the proposed experiment for a measurement of the non-linear phase shift in a QPG. A Michelson-like interferometer with a two-photons input state $|1_R\rangle|1_B\rangle$, *probe* and *trigger*, respectively, allows to measure the non-linear phase induced by the XPM on the logical basis of the qubits, which coincide with the two lowest Fock states. Two intense classical fields α_t (*tuner* with Rabi frequency Ω_1) and α_c (*coupler*, with Rabi frequency Ω_4), are necessary to the 5-level XPM process. L is a lens for the mode matching in the EIT medium. BS a 50/50 beam splitter. DL a delay line. FP_{1,2} Fabry-Perot cavities. D_{R,B1,B2} are avalanche-photodiodes APDs. *Left Inset* – Scheme using a Sagnac interferometer for avoiding the optical path difference. M is a mirror. *Right Inset* – Frequency spectrum for a 2 mm FP cavity length and finesse equal to 10^3 . The spectra of the probe and trigger photon are also shown in the plots as lines.

The interferometer is realized with the help of a 50/50 beam splitter (BS), using a Fabry-Perot cavities (FP_{1,2}) instead of mirrors. The FPs reflect back the probe field, which is then superimposed on the BS and detected by an APD (D_R), and transmit the trigger field detected by an APD in each arm (D_{B1} e D_{B2}). This implies that only the trigger frequency is resonant with the FPs’ cavity, which has a cavity length of 2 mm corresponding to a FSR of 74.85 GHz, while the probe frequency falls in the middle of the previous 93th and 94th FSRs. According to the photon bandwidth, a finesse of 10^3 determines a reflectivity for the probe field of 99.9% (see the spectra in the *Right Inset* of Fig. 12).

Since the frequency-bandwidths of the two photons are

well distinguished and the FPs filter out the trigger field, this apparatus determines an interferometer for the probe field only. The coincidence probabilities $P(R, B1)$, between D_R and D_{B1}, and $P(R, B2)$, between D_R and D_{B2}, post-select the events in which the trigger photon is. In this case the coincidence probabilities are equal and given by

$$P(R, B1) = P(R, B2) = [1 + \cos \Phi]/8 \quad (21)$$

where Φ represents the phase difference due to the different optical paths of the two arms experienced by the probe. In arm 2 a delay line (DL) is added to compensate the difference in the optical path and to scan for the interference pattern. In the *Left Inset* of Fig. 12 a Sagnac-like version of the interferometer is shown, which allows for an auto-compensation of the optical path delay as the two arms coincide.

When an EIT-based XPM system is considered in one arm, say arm 1, a non-linear contribution to the phase is added by the QPG, whether the trigger photon is present in the arm 1 or not. The XPM requires two intense classical fields resonant to the $D_2F = 1 \rightarrow F' = 1$ (384.232 THz) and $D_1F = 1 \rightarrow F' = 1$ (377.235 THz), σ^- circularly polarized tuner field (α_t , Ω_1), and σ^+ circularly polarized coupling field (α_c , Ω_4), respectively. The coincidence probabilities $P(R, B1)$, between D_R and D_{B1}, and $P(R, B2)$, between D_R and D_{B2}, enable post-selection of the events in which the trigger photon is in the arm 2 and hence the interference pattern is given by Eq. (21). Instead a non-linear contribution to the phase is expected when detections on D_R are post selected by the detection on D_{B2}. Fig. 13 represents the diagram of the four amplitude probabilities after the action of the BS and the FPs on the two-photons state. The non-linear phase ϕ_{11} is added only to the first diagram.

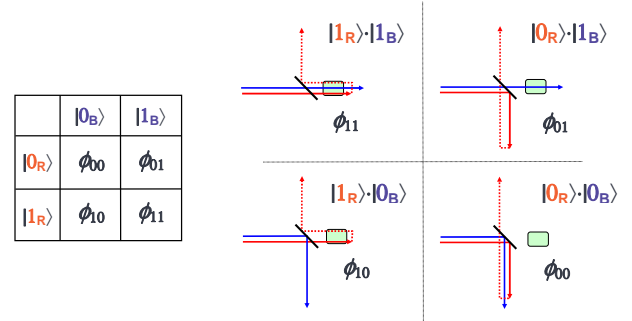


FIG. 13: Truth-table of the QPG for a logical basis of the qubits determined by the two lowest Fock states. On the right, diagrams corresponding to the probability amplitudes after the action of the BS and the FPs on the two-photons input state are shown.

According to the truth-table and the amplitudes of Fig. 13, the coincidence probabilities can be evaluated

to be

$$P(R, B1) = [1 + \cos(\tilde{\Phi} + \phi)]/8 \quad (22)$$

$$P(R, B2) = [1 + \cos \tilde{\Phi}]/8 \quad (23)$$

with $\tilde{\Phi} = \Phi + (\phi_{10} - 2\phi_{00} + \phi_{+0})$. ϕ_{+0} is the phase due to the probe photon reflected in arm 1 with ‘wrong’ σ^+ circular polarization. The phases ϕ_{10} and ϕ_{00} have been introduced in Eq. (1) as well as the conditional phase shift $\phi = \phi_{11} - \phi_{01} - \phi_{10} + \phi_{00}$ of the QPG. The phase difference between the two interference patterns determined by the two coincidence probabilities determines univocally the value of ϕ . In the case of an ideal QPG for which $\phi = \pi$ the two coincidence probabilities have opposite phases.

Polarization logical basis – The previous proposal indirectly tests the QPG based on the XPM detecting the non-linear phase shift by a Michelson interferometer and coincidence measurements. A direct measurement of the truth table or a test on a general qubit state requires a control and measurement of a superposition of vacuum and one photon state. While the generation of a superposition of vacuum and single photon state has been already achieved [21], the measurement of such a superposition requires also a homodyne measurement [24, 25]. However a logical basis for the qubits can be chosen as the circular polarization basis of the probe and trigger photons. A test of the QPG will then require the detection of both photons thus avoiding a problematic production and detection of Fock state superpositions.

The experimental setup is the same as in Fig. 12, but the qubits are now encoded in the polarization of the input two-photon state. According to the truth-table and

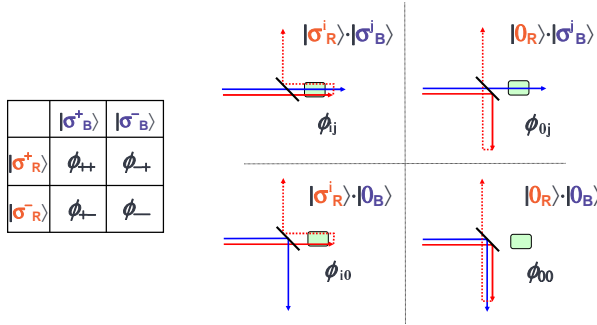


FIG. 14: Truth-table of the QPG for a logical basis of the qubits determined by orthogonal circular polarization basis. On the right the diagrams corresponding to the probability amplitudes after the action of the BS and the FPs on the two-photons input state.

the amplitudes in Fig. 14 it is possible to derive the coincidence probabilities $P(R_i, B1_j)$ and $P(R_i, B2_j)$, with $i, j = \{+, -\}$, as

$$P(R_i, B1_j) = [1 + \cos(\overline{\Phi} + \overline{\phi}_{ij})]/8 \quad (24)$$

$$P(R_i, B2_j) = [1 + \cos \overline{\Phi}]/8 \quad (25)$$

with $\overline{\Phi} = \Phi + (\phi_{i0} - 2\phi_{00} + \phi_{(i\oplus 1)0})$, where $i \oplus 1$ is the sum mod 2. The phase $\overline{\phi}$ is now given as $\overline{\phi}_{ij} = \phi_{ij} - \phi_{i0} - \phi_{0j} +$

ϕ_{00} , where ϕ_{i0} is the phase due to the EIT for the probe photon with polarization i and no trigger photon present, and same meaning for the other phases. Note that for $i = j = '-' \equiv '1'$ one obtains the previous expression for the QPG phase in the logical Fock-state basis. Four possible choices of the probe and trigger polarizations determine the phases

$$\begin{aligned} \overline{\phi}_{--} &= \phi_{--} - \phi_{-0} - \phi_{0-} + \phi_{00} \\ \overline{\phi}_{-+} &= \phi_{-+} - \phi_{-0} - \phi_{0+} + \phi_{00} \\ \overline{\phi}_{+-} &= \phi_{+-} - \phi_{+0} - \phi_{0-} + \phi_{00} \\ \overline{\phi}_{++} &= \phi_{++} - \phi_{+0} - \phi_{0+} + \phi_{00}, \end{aligned} \quad (26)$$

which satisfies the relation $\overline{\phi}_{--} - \overline{\phi}_{-+} - \overline{\phi}_{+-} + \overline{\phi}_{++} = \phi_{--} - \phi_{-+} - \phi_{+-} + \phi_{++} = \phi$. In the case of an ideal EIT for which $\phi_{+0} = \phi_{0+} = \phi_{++} = \phi_{00}$, $\phi_{-+} = \phi_{-0} = \phi_R$ and $\phi_{+-} = \phi_{0-} = \phi_B$, where $\phi_{A,B}$ are the phases acquired by the single photons, we have $\overline{\phi}_{--} = \phi$, and $\overline{\phi}_{-+} = \overline{\phi}_{+-} = \overline{\phi}_{++} = 0$. In a way the phases between the two coincidence interference patterns allow a measurement of the QPG phases in the diagonal basis, i.e. in the single qubit states for which the only non zero phase shift is the conditional phase shift ϕ of the QPG.

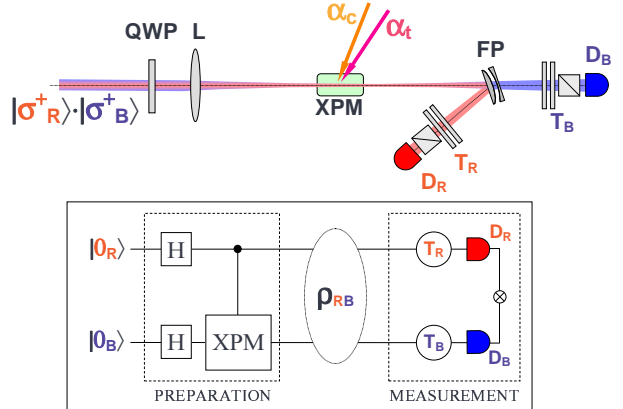


FIG. 15: Scheme of the proposed experiment for a complete characterization of the QPG. Two photons in the σ^+ polarization state (logical state $|0_R\rangle \otimes |0_B\rangle$) are transformed by a QWP, corresponding to two Hadamard single-qubit gates, and then to the XPM medium (QPG). A Fabry-Perot cavity with the same parameter as before transmits the trigger photon and reflect the probe to two tomographic measurement systems ($T_{R,B}$) and detected by APDs.

General polarization qubit input states – The polarization logical basis allows for a direct observation of coherence and production of entanglement as necessary conditions for a QPG. Assume that the information is encoded in the polarization state of two photons, and then sent into the EIT-based XPM system for QPG, as shown in Fig. 15. The output photons, as shown in Fig. 15, are split by a dichroic mirror (a tilted FP cavity with the same parameters as before) and then collected in two APDs (D_R and D_B) for coincidence counting. In front of each detector a tomographic system [26] constituted by

a QWP, HWP and a PBS, is placed for the complete reconstruction of the polarization state of the output, thus providing the information on coherence properties of the gate. It has also been shown [3] that an input state for the QPG given by $[(|\sigma_R^+\rangle + |\sigma_R^-\rangle) \otimes (|\sigma_B^+\rangle + |\sigma_B^-\rangle)]/2$ can quantify the entanglement of the output state, for which the CHSH inequality is $2\sqrt{1 + \sin^2 \phi}$ where 2 is the upper classical limit.

VII. CONCLUSION

In conclusion, our study shows that the implementation of efficient EIT-based nonlinear two-qubit gates for travelling single-photons is possible, even though experimentally challenging. The main limitation is due to the existence of a trade-off between the size of the CPS and the fidelity of the gate, limiting the achievable gate fidelity in the stationary regime, but which can be partially bypassed in the transient regime. Since this trade-off is a general consequence of the coherent interaction between the atomic medium and the single-photon wave-

packets, we expect that these considerations apply to all EIT-based crossed-Kerr schemes [10, 11], regardless the specific level scheme considered. Instead, this consideration does not apply to situations where the nonlinearity comes from independent processes (e.g. collisions of dipole-dipole interactions) [14], nor the similar solid-state based processes [23].

VIII. ACKNOWLEDGEMENTS

This work has been partly supported by the European Commission through FP6/2002/IST/FETPI SCALA: Scalable Quantum Computing with Light and Atoms, Contract No 015714, CONQUEST network, MRTN-CT-2003-505089 and under the Integrated Project Qubit Applications (QAP) funded by the IST directorate, Contract No 015848. GDG also acknowledges financial support from the Ministero della Istruzione, dell'Università e della Ricerca (PRIN-2005024254 and FIRB-RBAU01L5AZ).

[1] I. L. Chuang and Y. Yamamoto, Phys. Rev. A **52**, 3489 (1995).

[2] E. Knill, R. Laflamme and G. J. Milburn, Nature (London) **409**, 46 (2001).

[3] Q.A. Turchette *et al.*, Phys. Rev. Lett. **75**, 4710 (1995); A. Rauschenbeutel *et al.*, *ibid.* **83**, 5166 (1999).

[4] E. Arimondo, in *Progress in Optics XXXV*, ed. by E. Wolf, (Elsevier, Amsterdam, 1996); S. E. Harris, Physics Today **50**(7), 36 (1997); M. D. Lukin and A. Imamoğlu, Nature (London) **413**, 273 (2001);

[5] M. Fleischhauer, A. Imamoğlu and J. Marangos, Rev. Mod. Phys. **77**, 633 (2005).

[6] H. Schmidt and A. Imamoğlu, Opt. Lett. **21**, 1936 (1996).

[7] H. Wang, D. Goorskey and M. Xiao, Phys. Rev. Lett. **87**, 073601 (2001); H. Kang and Y. Zhu, Phys. Rev. Lett. **91**, 093601 (2003).

[8] J.-F. Roch *et al.*, Phys. Rev. Lett. **78**, 634 (1997); P. Grangier *et al.*, Phys. Rev. Lett. **81**, 2833 (1998).

[9] A. B. Matsko *et al.*, Phys. Rev. A **67**, 043805 (2003); A. B. Matsko *et al.*, Opt. Lett. **28**, 96 (2003); A. D. Greentree *et al.*, Phys. Rev. A **67**, 023818 (2003).

[10] M. D. Lukin and A. Imamoğlu, Phys. Rev. Lett. **84**, 1419 (2000).

[11] C. Ottaviani *et al.*, Phys. Rev. Lett. **90**, 197902 (2003).

[12] D. Petrosyan and G. Kurizki, Phys. Rev. A **65**, 033833 (2002).

[13] S. Rebić *et al.*, Phys. Rev. A **70**, 032317 (2004); D. Petrosyan and Y. P. Malakyan, Phys. Rev. A **70**, 023822 (2004).

[14] M. Mašalas and M. Fleischhauer, Phys. Rev. A **69**, 061801(R) (2004); I. Friedler, G. Kurizki and D. Petrosyan, Phys. Rev. A **71**, 023803 (2005); A. Andrè *et al.*, Phys. Rev. Lett. **94**, 063902 (2005).

[15] S. Lloyd, Phys. Rev. Lett. **75**, 346 (1995).

[16] M. A. Nielsen and I. L. Chuang, *Quantum Computation and Quantum Information*, (Cambridge University Press, Cambridge 2000.)

[17] C. Ottaviani, S. Rebić, D. Vitali, and P. Tombesi, Phys. Rev. A **73**, 010301(R) (2006).

[18] L.-M. Duan, J. I. Cirac, and P. Zoller, Phys. Rev. A **66**, 023818 (2002).

[19] L. M. Duan, M. D. Lukin, J. I. Cirac and P. Zoller, Nature (London) **414**, 413 (2001); J. I. Cirac, L. Duan and P. Zoller, in *Experimental Quantum Computation and Information*, ed. by F. De Martini and C. Monroe, (IOS Press, Amsterdam 2002.), also available as e-print quant-ph/0405030.

[20] J. F. Poyatos, J. I. Cirac and P. Zoller, Phys. Rev. Lett. **78**, 390 (1997).

[21] B. Darquié, M. P. A. Jones, J. Dingjan, J. Beugnon, S. Bergamini, Y. Sortais, G. Messin, A. Browaeys and P. Grangier, Science **309**, 454 (2005).

[22] H. J. Carmichael, *An Open Systems Approach to Quantum Optics*, Lecture Notes in Physics, (Springer, Berlin, 1993.)

[23] J. J. Longdell *et al.*, Phys. Rev. Lett. **93**, 130503 (2004); E. Fraval *et al.*, Phys. Rev. Lett. **92**, 077601 (2004); J. J. Longdell *et al.*, Phys. Rev. Lett. **95**, 063601 (2005); E. Fraval *et al.*, Phys. Rev. Lett. **95**, 030506 (2005).

[24] A. Zavatta, S. Viciani and M. Bellini, Science **306**, 660 (2004).

[25] S. A. Babichev, B. Brezger and B. Lvovsky, Phys. Rev. Lett. **92**, 047903 (2004).

[26] D. F. V. James, P. G. Kwiat, W. J. Munro and A. G. White Phys. Rev. A **64**, 052312 (2001).

[27] Without the dephasing, steady-state fidelities reach the values of 77% and 83% for unconditional and conditional cases, respectively